Geochemistry Geophysics Geosystems G3

*Article*
Volume 13, Number 7
14 July 2012
Q07007, doi:10.1029/2012GC004158
ISSN: 1525-2027

Published by AGU and the Geochemical Society

# Fluid and gas fluxes from the Logatchev hydrothermal vent area

**Oliver Schmale**
*Leibniz Institute for Baltic Sea Research Warnemünde, DE-18119 Rostock, Germany (oliver.schmale@io-warnemuende.de)*

**Maren Walter**
*Institute for Environmental Physics, University of Bremen, DE-28359 Bremen, Germany*

**Jens Schneider von Deimling**
*GEOMAR, Helmholtz Centre for Ocean Research Kiel, DE-24148 Kiel, Germany*

**Jürgen Sültenfuß**
*Institute for Environmental Physics, University of Bremen, DE-28359 Bremen, Germany*

**Sharon Walker**
*National Oceanic and Atmospheric Administration, Seattle, Washington 98115, USA*

**Gregor Rehder**
*Leibniz Institute for Baltic Sea Research Warnemünde, DE-18119 Rostock, Germany*

**Robin Keir**
*GEOMAR, Helmholtz Centre for Ocean Research Kiel, DE-24148 Kiel, Germany*

[1] The Logatchev hydrothermal field at 14°45′N on the MAR is characterized by gas plumes that are enriched in methane and helium compared to the oceanic background. We investigated $CH_4$ concentration and $\delta^{13}C$ together with $\delta^3He$ in the water column of that region. These data and turbidity measurements indicate that apart from the known vent fields, another vent site exists northeast of the vent field Logatchev 1. The distribution of methane and $^3He$ concentrations along two sections were used in combination with current measurements from lowered acoustic Doppler current profilers (LADCP) to calculate the horizontal plume fluxes of these gases. According to these examinations 0.02 $\mu$mol $s^{-1}$ of $^3He$ and 0.21 mol $s^{-1}$ of methane are transported in a plume that flows into a southward direction in the central part of the valley. Based on $^3He$ measurements of vent fluid (22 $\pm$ 6 pM), we estimate a total vent flux in this region of about 900 L $s^{-1}$ and a total flux of $CH_4$ of 3.2 mol $s^{-1}$.

**Components:** 6200 words, 8 figures.

**Keywords:** Mid-Atlantic Ridge; helium; hydrothermal; hydrothermal fluxes; methane; plumes.

**Index Terms:** 3017 Marine Geology and Geophysics: Hydrothermal systems (0450, 1034, 3616, 4832, 8135, 8424); 4512 Oceanography: Physical: Currents; 4808 Oceanography: Biological and Chemical: Chemical tracers; 4820 Oceanography: Biological and Chemical: Gases; 4870 Oceanography: Biological and Chemical: Stable isotopes (0454, 1041).

**Received** 21 March 2012; **Revised** 11 June 2012; **Accepted** 11 June 2012; **Published** 14 July 2012.

Schmale, O., M. Walter, J. Schneider von Deimling, J. Sültenfuß, S. Walker, G. Rehder, and R. Keir (2012), Fluid and gas fluxes from the Logatchev hydrothermal vent area, *Geochem. Geophys. Geosyst.*, *13*, Q07007, doi:10.1029/2012GC004158.

## 1. Introduction

[2] The Mid-Atlantic Ridge (MAR) is a slow-spreading ridge on which mantle (ultramafic) rock outcrops in places due to the extensional tectonics [*Aumento and Loubat*, 1971; *Cannat et al.*, 1995, 1997; *Dick*, 1989]. Some of these places are characterized by fold-systems that favor the circulation of fluids in the subsurface with focused or diffuse fluid-release at the seafloor [*Petersen et al.*, 2009]. The composition of these fluids depends on the geological, petrological and temperature regime; the fluid chemistry can also be modified by biotic or abiotic reactions in the subsurface. Dissolved metals like iron and manganese that are transported by the fluid discharge into the water column are oxidized and form particles that influence the turbidity of the plume water [*Marbler et al.*, 2010]. Most of the hydrothermal fluids show methane and $^{3}$He concentrations that are enriched compared to the surrounding water column. In the case of methane, different source mechanisms are discussed in the literature: (1) primordial methane released from the mantle [*Welhan*, 1988]; (2) methane produced by thermogenic reactions from organic matter [*Welhan*, 1988], and (3) methane created by serpentinization of ultramafic rock [*Charlou et al.*, 1998]. The stable isotope ratio of hydrothermal methane shows a strong enrichment in $^{13}$C ($\delta^{13}$C values on the Mid-Atlantic Ridge axis varies between $-7$ and $-19$‰) compared to the isotope signature in the background seawater ($\delta^{13}\mathrm{C} \approx -35$‰ [*Keir et al.*, 2009]). In the case of $^{3}$He, it is known that magma production at the MAR accounts for the positive $^{3}$He anomaly that can be found in the Atlantic deep water [*Rüth et al.*, 2000]. $^{3}$He was trapped in the mantle during the accumulation of the earth's crust and is constantly degassed by volcanism.

[3] After the release of hydrothermal effluent at the seafloor, the ascending fluids are diluted by entrainment of ambient seawater. The plume rise height depends on the physical characteristics of the vent fluid as well as the hydrographic situation. After the plume has reached a water depth of zero buoyancy it spreads horizontally in the effluent layer. Despite vigorous dilution, methane and $^{3}$He are well enriched in the non-buoyant effluent layer compared to the ambient seawater. During the horizontal spreading of the plume the gas concentration decreases constantly. $^{3}$He is a conservative tracer; its plume-concentration is only influenced by physical processes and is not modified by any chemical or biological reaction. The concentration of methane is additionally influenced by microbial oxidation as it represents an important energy source for the microbes in the deep ocean. The faster consumption of $^{12}CH_4$ relative to that of $^{13}CH_4$ results in a constant increase of $\delta^{13}$C-$CH_4$ values in the aging plume waters [*Tsunogai et al.*, 2000; *Whiticar*, 1999]. Thus, methane in the core of the plume becomes isotopically heavier than in the hydrothermal source as the concentration decreases downstream. However, sharp vertical gradients toward isotopically light values develop above and below the plume where background methane from the open ocean mixes with the residual hydrothermal methane [*Keir et al.*, 2009].

[4] One hydrothermal vent area at the MAR that has been investigated in detail by different scientific disciplines is the Logatchev hydrothermal field (LHF [e.g., *Batuev et al.*, 1994; *Charlou et al.*, 2010; *Keir et al.*, 2009; *Petersen et al.*, 2011, 2009; *Schmidt et al.*, 2007]). The LHF is located between the Fifteen-Twenty and Marathon Fracture Zones and consists of four hydrothermal sites (LHF-1 to -4; Figure 1). These sites are roughly located along an east-southeast orientated line that starts at LHF-1 and ends after 9 km at LHF-4. Recent studies show that LHF-1 and -2 are actively releasing fluids into the water column and that LHF-3 and -4 are inactive [*Petersen et al.*, 2009]. It is hypothesized that the complex tectonic situation and the resulting fault systems control the distribution of the different vent sites [*Petersen et al.*, 2009]. LHF-1 at 14°45′N on the MAR is situated on a plateau at the eastern inner flank of the rift valley wall in water depths between 3060 to 2900 m and consists of at least seven active high- and low-temperature vent sites in a narrow NW-SE striking zone [*Petersen et al.*, 2009]. The hydrothermal field is one of a few known submarine hydrothermal systems associated with ultramafic rocks that have undergone different degrees of serpentinization [*Augustin et al.*, 2008]. This alteration leads to fluid compositions that are highly enriched in hydrogen (∼16 mM [*Charlou et al.*,

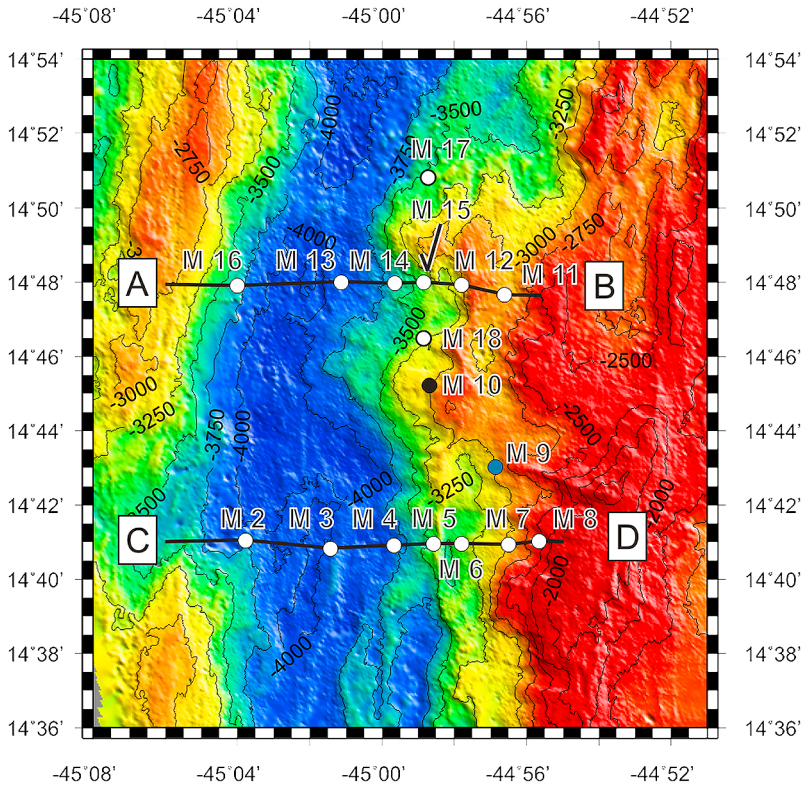


**Figure 1.** Station map of cruise M81–2c in the region of the Logatchev Hydrothermal Field. LHF-1 is located at station M10 (black dot), LHF-2 at station M9 (blue dot). The lines between A-B and C-D represent the northern and southern transects.

2002]), methane (~3 mM [*Schmidt et al.*, 2007]) and $^3$He (~30 pM [*Keir et al.*, 2009]). The $\delta^{13}$C value of vent fluid methane shows values of about −13‰ [*Keir et al.*, 2009]. The characteristic gas composition of this fluid together with turbidity anomalies that result from metal-precipitation can be traced over a broad distance in the rift segment [*Keir et al.*, 2009; *Marbler et al.*, 2010].

[5] Our goal in the present paper is to deliver a detailed view of the distribution pattern of methane, $\delta^{13}$C-$CH_4$ and $\delta^3$He in the water column surrounding the Logatchev hydrothermal field. The LADCP data will be used to describe the current regime and to estimate the fluxes of methane, $^3$He and the volume flow rate of the vent fluids.

## 2. Methods

[6] Water column samples were obtained during a scientific cruise in April 2010 on the German research vessel *Meteor* (cruise number M81–2c). All ship-based investigations were carried out in a three day time frame. The vertical hydrocasts were performed with a SBE911 plus CTD system that was mounted on a SBE32 carousel sampler equipped with 22 Niskin bottles (à 10 l). Current measurements were carried out with a lowered acoustic Doppler current profiler (LADCP) system, where two RDI 300 kHz Workhorse Monitor ADCPs mounted on the water sampling unit were used for full-depth current profiling in a master and slave setup. The vertical resolution was set to 10 m. The LADCP raw data have been processed with an inverse method [*Visbeck*, 2002] using barotropic, bottom track and smoothness constraints, as well as external pressure from the CTD system. The overall accuracy of the velocity data suffered to some extent from the paucity of scatters below 1500 m water depth. However, after a careful post-processing, screening of the data showed a very good agreement between casts, even for small scale features, resulting in a final single-point accuracy of less than 5 cm s$^{-1}$ error for the velocities. Uncertainties are further reduced for this study by using the average velocity within the plume layer (2300 to 3400 m water depth).

[7] A miniature autonomous plume recorder (MAPR [*Walker et al.*, 2004]) was attached on the frame of the carousel sampler to measure simultaneously the

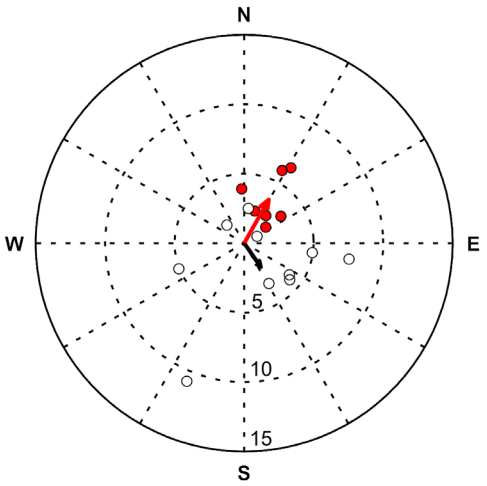


**Figure 2.** Scatter of detided current speed (numbers indicate speed in cm $s^{-1}$) and direction for water column profiles M2 through M18 for the plume layer average between 2300 and 3400 m for the individual stations within the rift valley on both sections (white dots) and on the slope (red dots). Arrows indicate the respective average velocity and direction.

optical backscatter on the vertical hydrocasts. Turbidity anomalies were expressed in ΔNTU, which is the difference in NTU (nephelometric turbidity units) between the plume water and the unaffected water above the plume level. The MAPR was also equipped with an ORP-sensor that analyzes the oxidation-reduction potential (ORP) of the plume relative to ambient seawater. Greater ΔNTU or ORP anomalies indicate "younger" or "fresher" parts of the plume, which are closer to the source [*Baker et al.*, 2010].

[8] Seawater for methane analysis was directly filled from the Niskin bottles into pre-evacuated 2-L sample bottles resulting in a partial degassing of the water. The gas phase was then recompressed to atmospheric pressure and the mole fraction of methane determined using a GC system equipped with a flame ionization detector. The overall error of the method depends on the methane concentration and varies between ±0.2 nM for $[CH_4] \leq 7$ nM and ±3% for $[CH_4] > 7$ nM [*Buller*, 2008; *Keir et al.*, 2009].

[9] The gas samples for stable isotope measurements of methane carbon ($\delta^{13}$C-$CH_4$) were taken by transferring a subsample of the extracted gas into pre-evacuated 20-ml vials. The isotope ratio was determined at the Leibniz Institute of Baltic Sea Research (IOW) using an inline ratio monitoring mass spectrometer [*Schmale et al.*, 2010]. The average precision of that method has been determined to be ±1‰.

[10] Water samples for helium isotope analyses were directly transferred from the Niskin bottles into pinched-off copper tubes. During a scientific cruise in 2007 on the German research vessel *Maria S. Merian* (cruise number MSM04–3) direct fluid samples from the vents at LHF-1 were collected in copper tubes and closed with stainless steel valves by the submerged ROV. Dissolved gases were extracted from the water and $^3$He and $^4$He concentrations were determined with a high resolution mass spectrometer (MAP 215–50) at the University of Bremen. The uncertainty of the $^3$He/$^4$He ratio is 0.5% [*Sültenfuß et al.*, 2009]. Because Ne has no sources in the ocean, Ne was also analyzed to identify the atmospheric contamination of the samples.

## 3. Results and Discussion

### 3.1. Horizontal Flow Field

[11] The directly measured flow field at LHF represents a snapshot during the time of the measurement campaign. Nevertheless, for the time span covered by the measurements (3 days), a consistent picture of the flow field emerges. The field is a superposition of periodic tidal currents and the residual background flow. The tidal component of the flow is not instrumental in the large scale mean plume advection, so we attempt to extract the mean flow by removing the tidal component. Since no long-term current measurements are available at LHF for a direct determination of the amplitude and phase of the local tides, barotropic tidal currents were determined with the TPXO7.1 tidal model [*Egbert and Erofeeva*, 2002]. The tide in the area of the LHF is predominantly semidiurnal, with $M_2$ as the major constituent. The major axis of the tidal ellipse is orientated in SSE direction, along the axial graben. The amplitude of the modeled tidal currents is on average less than 3 cm $s^{-1}$.

[12] The residual background flow in the non-buoyant plume layer between 2300 and 3400 m depth can be separated into a broad, weak, southward flow within the rift valley, and a more focused northward flow along the slope of the eastern sidewall, where the vents are located (Figures 2 and 3). The scatter in velocity speed and direction between the individual stations on the two sections within the rift valley is of the same order of magnitude as the mean (and the tides), but the total mean for those stations is nevertheless clearly oriented in the southward direction (average velocity for the rift valley of 2.1 cm $s^{-1}$ in south-southeast direction,

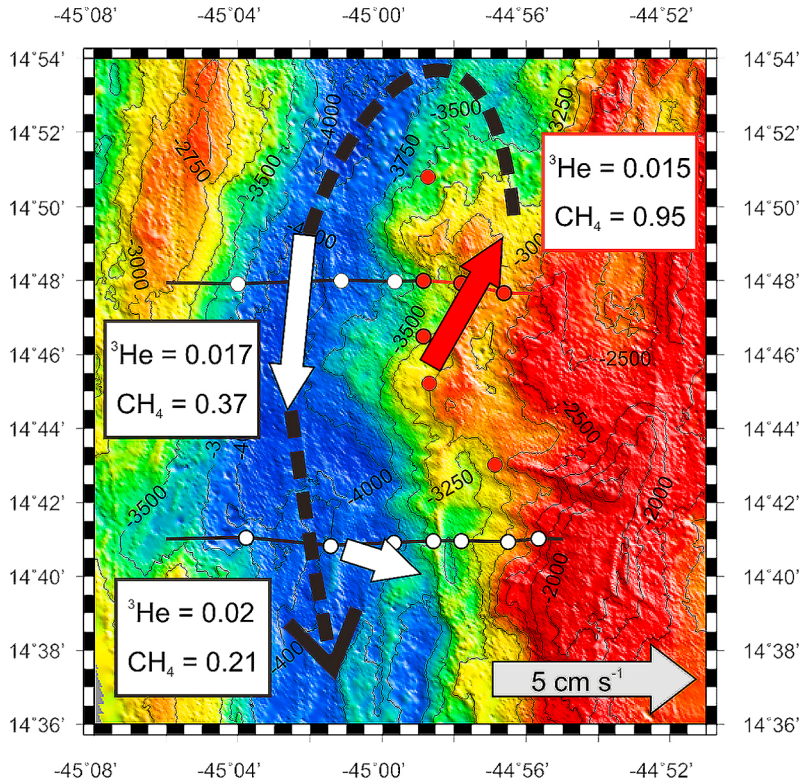


**Figure 3.** Current field at LHF. The current velocity is averaged in a depth range between 2300 and 3400 m (a scale is displayed with the gray arrow). The white dots represent the stations that were used to calculate the current velocities for the northern and southern section within the main valley, respectively (white arrows). The red dots mark the stations that represent the slope current (red arrow). The boxes show the $^3$He and $CH_4$ fluxes through the different sections (note the different units for $^3$He in $\mu$mol s$^{-1}$ and $CH_4$ in mol s$^{-1}$). The black dotted arrow indicates the supposed horizontal plume circulation.

Figure 2). The average velocity within the valley across the northern section is 4.3 cm s$^{-1}$ to the south. The average current across the southern section is lower (2 cm s$^{-1}$) with a more easterly component (Figure 3). The average velocity of the northeastward along-slope current is 3.6 cm s$^{-1}$, and appears to be more directed, following the topography (Figure 3). This northward direction of the flow at the LHF-1 vent site is consistent with observations of plume bending during ROV deployments on earlier cruises [*Marbler et al.*, 2010]. A prevailing southward direction for the flow within the rift valley is supported by the large scale along valley density gradient (not shown). For these reasons, we will in the following assume that the snapshot of the horizontal circulation is at least to some extent representative of the general circulation in the vicinity of the Logatchev field, with prevailing northward currents on the slope at the locations of LHF-1 and LHF-2, and a sluggish southward flow in the axial valley (Figure 3). We will interpret the measured plume signals in the context of these observations.

## 3.2. Turbidity Above Hydrothermal Vents

[13] MAPR investigations during the time of the measurement campaign clearly indicate vent activity at three sites in the vicinity of the Logatchev vent area. Turbidity anomalies recorded directly above LHF-1 indicate the "split-level" structure of the hydrothermal plume (Figure 4) that was already observed in previous water column studies at this location [*Marbler et al.*, 2010]. The specific structure is also reflected by the vertical distribution of methane and $\delta^3$He ($CH_4$ maxima at 2760 and 2910 m water depth, Figure 5) and negative ORP anomalies (maxima at 2660 and 2980 m water depth, data not shown). It has been suggested, that the diverse plume levels can be explained by different compositions of vent fluids that are influencing the density and therefore the buoyancy of the plume [*Sudarikov and Roumiantsev*, 2000]. They suggest that the near-bottom plume (reverse plume) results from fluids that contain brine due to vapor-liquid phase separation in the hydrothermal circulation. However, such a specific fluid composition that shows enhanced

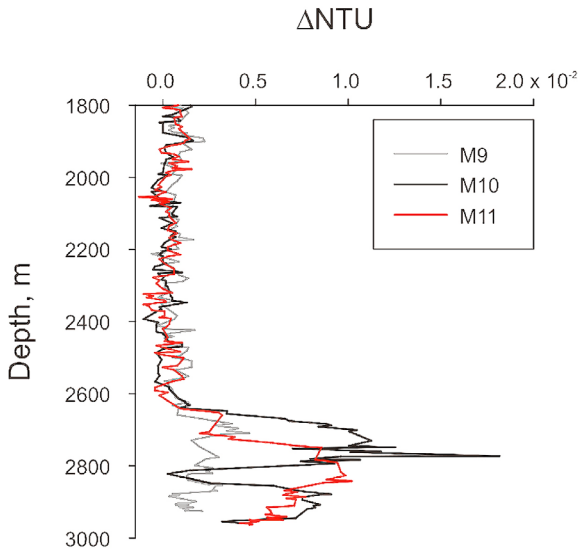


**Figure 4.** Vertical turbidity profiles (ΔNTU) at stations M9 (LHF-2), M10 (LHF-1) and M11.

chloride concentrations could neither be identified for LHF-1 [*Schmidt et al.*, 2007] nor for LHF-2 [*Fouquet et al.*, 2008]. Another factor that can contribute to the observed layered plumes is variable current speeds, either in the background flow, or over the tidal cycle [*Di Iorio et al.*, 2012; *Walter et al.*, 2010]. The strength of the current affects the entrainment of ambient seawater into the rising plume; in a strong flow the entrainment is stronger and reduces the maximum rise height. MAPR investigations above LHF-2 show that the water column directly above that vent site is also characterized by turbidity anomalies, that are much weaker compared with the signal recorded above LHF-1 (Figure 4). This is consistent with previous measurements that show that LHF-2 vent fluids are much less enriched in metal concentrations than at LHF-1 [*Charlou et al.*, 2010].

[14] Our MAPR investigations indicate additional vent activity near station M11 that was not described in previous studies (Figure 4). The pronounced ΔNTU signal observed below 2600 m is comparable with the signal intensity measured at LHF-1 and may be due to nearby hydrothermal fluid release. ORP records on that water cast do not show any anomaly (data not shown), however, $\delta^3$He and $CH_4$ data support the presence of an additional vent field (section 3.3 below).

### 3.3. Distribution of $^3$He, Methane, and Methane $\delta^{13}$C

[15] Comparison of the gas data obtained from the cruise *Meteor* 81–2c with those from previous expeditions on R/V *M.S Merian* 4/3 (23 January to 14 February 2007 [*Keir et al.*, 2009]) and R/V *L'Atalante* (4 December 2007 to 2 January 2008 [*Keir et al.*, 2009]) indicates that the data sets from all three cruises are consistent. A plot of methane concentration versus $\delta^3$He shows a similar pattern to the data obtained on the previous expeditions (Figure 6). There appears to be a linear correlation between the higher values. As a result of microbial methane oxidation, at low $\delta^3$He values, the methane concentrations are often lower than expected from end-member mixing between background seawater ([$CH_4$] = 0.5 nM, $\delta^3$He = 3%) and enriched concentrations in the plume (line in Figure 6).

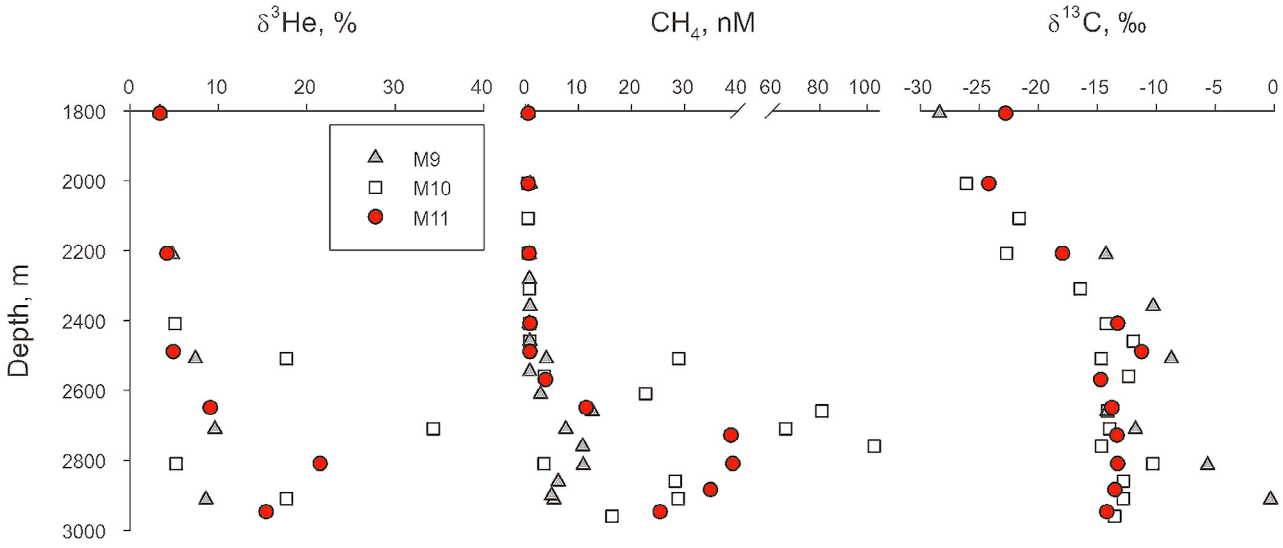


**Figure 5.** Vertical distribution of $\delta^3$He, $CH_4$ and $\delta^{13}$C $CH_4$ at stations M9 (LHF-2), M10 (LHF-1) and M11.

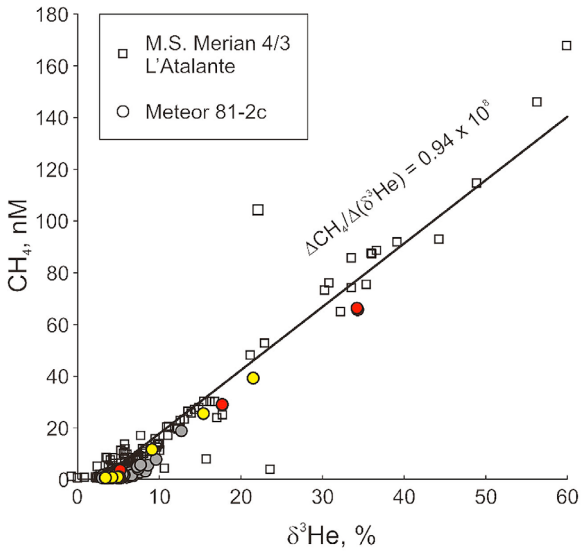


**Figure 6.** $CH_4$ concentration versus $\delta^3$He from *M.S Merian* 4/3 and *L'Atalante* (squares) [*Keir et al.*, 2009], and *Meteor* 81–2c (circles). The red circles indicate station M10 (LHF-1) and yellow circles M11. The line is anchored at $\delta^3$He = 3%, [$CH_4$] = 0.5 nM and visually fit to the trend of the high concentrations. The slope corresponds to a $^3$He/$CH_4$ mole ratio of $0.9 \times 10^8$ (calculated according to *Keir et al.* [2008]).

[16] During Meteor cruise M81–2c, most of the stations were positioned on two west-east lines across the rift valley, one north of LHF-1, and the other south of this vent field (Figure 1). The two transects were positioned perpendicular to the supposed main flow axis of the hydrothermal plume within the rift valley. The sections displayed in Figure 7 show hydrothermal plume signatures extend across the entire width of the rift valley. However, the diverse gas data sets reveal distinct hydrothermal plume structures. Along the $^3$He sections the hydrothermal plume appears as a "split-level" structure that could result from an intrusion of an external water body, an assumption that is not supported by the characteristics of the methane concentration and $\delta^{13}$C-$CH_4$ distribution pattern. Another explanation for this specific plume structure could be a fluid release from different water depths. LHF-1 is located in about 3000 m water depth whereas LHF-2 is situated in a depth of about 2700 m. At least for the southern section that is very close to LHF-2 one could assume that LHF-1 might be responsible for the deep $^3$He plume whereas LHF-2 could be the source for the shallower plume signal. The methane concentration shows a plume center at about 2900 m water depth whereas the stable isotope data shows a center that is located about 200 m deeper. At the upper and lower plume boundaries the decreasing methane concentration and the lighter values of $\delta^{13}$C-$CH_4$ point to mixing with non-plume deep water. As described by *Keir et al.* [2009], the regional methane gas distribution in that area is influenced by mixing and microbial oxidation that leads to decreasing methane concentrations and $^{13}$C-$CH_4$ enrichment within the plume with increasing distance from the vent field. The microbial induced fractionation mechanism is clearly displayed by the stable carbon isotope values in our two sections placed almost equidistant to LHF-1 (Figure 7). The $\delta^{13}$C-$CH_4$ values identified in the plume centers of both the northern (+3.1‰ at M13 in 3130 m) and southern sections (+8.0‰ at M3 in 3131 m) are strongly enriched in $^{13}$C-$CH_4$ compared with the source signature of LHF-1 (about −14‰ at station M10, Figure 6). Assuming that the $^{13}$C-$CH_4$ enrichment is related to the transport distance of the plume, the stronger enrichment in the southern section may indicate that the plume is older here, hence has "aged" over a longer distance compared to the plume crossing the northern section. This consideration is supported by our interpretation of the horizontal flow field in the vicinity of the Logatchev area (section 3.1). It appears that the plume originates at the eastern slope (e.g., LHF-1) and is first transported northward by the slope current. Subsequently, the flow turns anticlockwise and the plume is carried southward with the main current within the rift valley (Figure 3). Consequently, the rift valley plume would first pass the northern and subsequently the southern section. This plume circulation is also supported by the distribution pattern of $CH_4$ concentration and $\delta^{13}$C-$CH_4$ in the northern section which shows regionally confined anomalies in the central part of the section (M13 and M14 between 2800 and 3300 m) that are separated from the slope anomalies (M12 between 2600 and 3000 m; Figure 7). The slope anomalies are characterized by high $CH_4$ concentrations together with relatively lighter $\delta^{13}$C-$CH_4$ values indicating a relatively "fresh" plume. In contrast, the anomalies in the central part of the northern section are characterized by relatively low methane concentrations and heavy $\delta^{13}$C-$CH_4$ values, suggesting an "aged" plume which has undergone microbial oxidation and isotopic fractionation.

[17] Apart from these general patterns, the gas data set indicates that LHF-2 is also actively releasing vent fluids into the water column, as observed by *Fouquet et al.* [2008] (Figure 5). Furthermore, an additional vent field appears to exist near station M11, 5 km to the northeast of

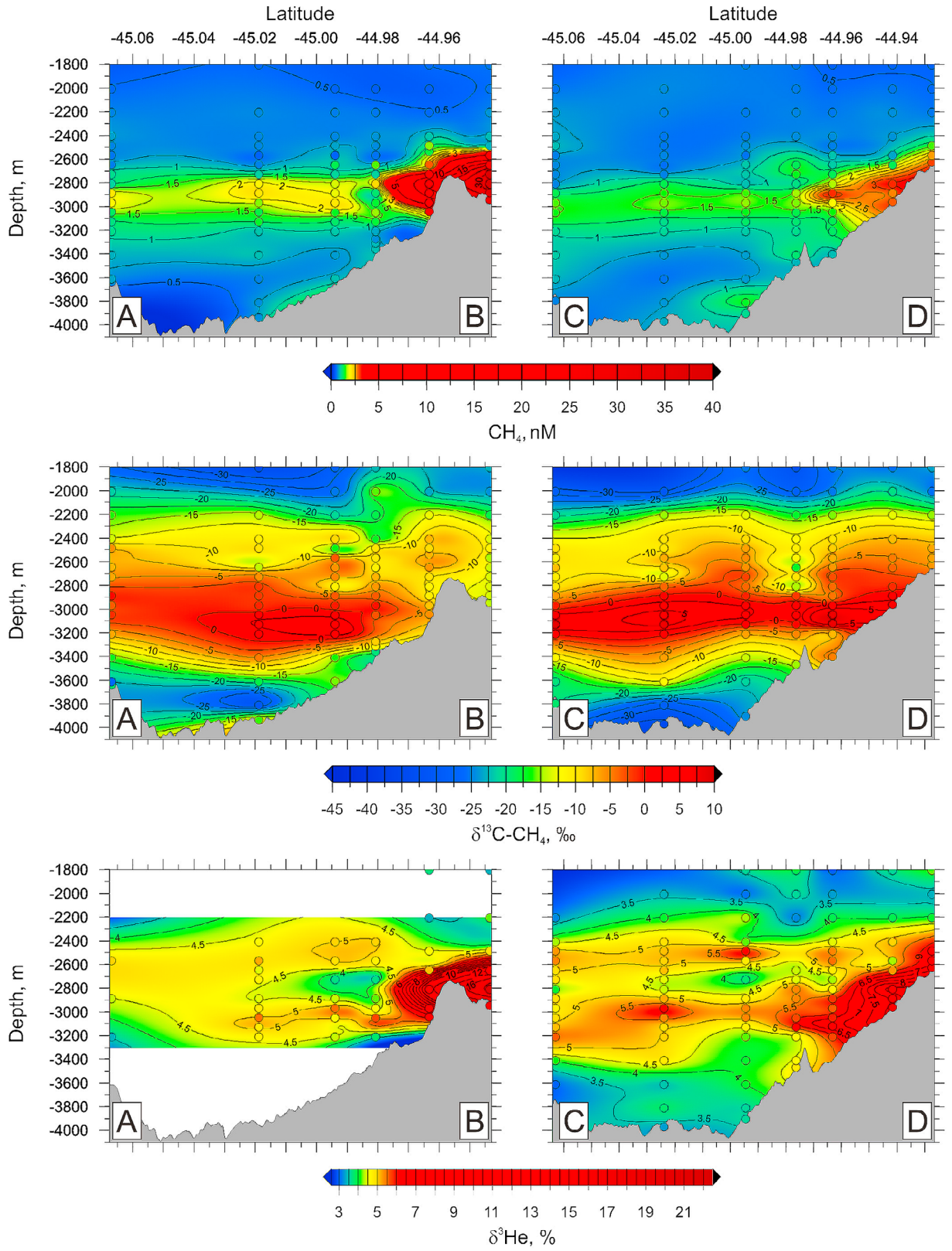


**Figure 7.** Gas distribution along the northern (left, A–B) and the southern transect (right, C–D). Methane concentration is displayed at the top, the stable carbon isotope ratio of methane carbon ($\delta^{13}$C $CH_4$) in the middle, and the $\delta^3$He distribution at the bottom.

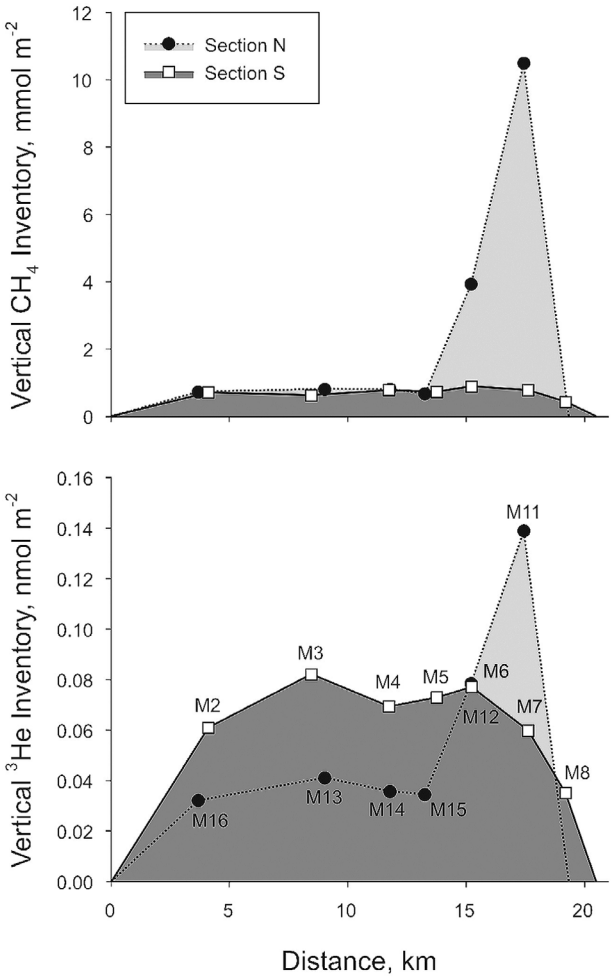


**Figure 8.** Vertical inventories of methane (top) and $^3$He (bottom) along the northern and southern sections.

LHF-1, as indicated by our MAPR investigation (see section 3.2). High methane concentrations and $\delta^3$He values of up to 39 nM and 21.5%, respectively, were measured at this site (Figures 5 and 7). A "young age" for the plume above M11 is suggested by the $\delta^{13}$C-CH$_4$ values of about −14‰ detected in the bottom waters, a value that is very similar to the source signature of near-field plume measurements at LHF-1 (Figure 5, station M10). The linear correlation of methane versus $\delta^3$He at Station M11 also is similar to that found at LHF-1 (Figure 6). By contrast, the $^{13}$C-CH$_4$ enrichment in the central part of the valley along the northern section (Figure 7) strongly indicates an "aged" plume that is distinctly separated from the signal at M11. The vent field presumed near station M11 is located in a valley that is separated from the main valley by a ridge inhibiting direct hydrological contact to LHF-1. The morphology at LHF-1 and that at this newly discovered vent area show some noticeable similarities (Figure 1). The morphology of the rift flank at these sites is characterized by W-E orientated swells that may be caused by the regional fault system. There are crosscutting tectonic faults at both LHF-1 and the region near M11 that may foster hydrothermal circulation [*Petersen*, 2006; *Petersen et al.*, 2009].

## 3.4. Horizontal Plume and Vent Fluxes

### 3.4.1. Horizontal Plume Flux of $^3$He and Methane

[18] Based on the information of the flow field and the gas distribution, we estimate the horizontal plume fluxes of $^3$He and methane in the region of LHF. We calculated the vertical inventories of both gases along the northern and southern sections (Figure 1). The background concentrations of methane (0.5 nM) and $\delta^3$He (3%) in the rift valley above the influence of the neutrally buoyant plume (at 1800 m water depth) were subtracted from the measured values to obtain the excess of these gases. Excess inventories were then calculated using the trapezoid method [*Keir et al.*, 2008]. The inventory of methane was integrated within a depth range of 2000 m to the bottom of the different stations for both sections. For the southern section, the calculation of the inventory of $^3$He was performed in an analogous manner, starting at a water depth of 2400 m. Because of the limited number of samples that could be taken for helium analyses at the northern transect, we only integrated the $^3$He inventory in a 2400–3200 m depth range. However, this depth-interval covers the plume depth and includes the main $^3$He excess (Figure 7). The different inventories were plotted as a function of distance along the two east-west lines starting at Longitude 45°06′W, assuming that the inventories at both ends of each section drop to zero (Figure 8).

[19] The cross-section inventories of methane obtained from this procedure are 39 mol m$^{-1}$ in the northern section and 12 mol m$^{-1}$ in the southern section. Except for the strong influence of the supposed vent area near station M11 on the section inventory in the north, the areal distribution of the two inventories look very similar. The $^3$He inventories for the two sections are 0.9 $\mu$mol m$^{-1}$ in the north and 1.2 $\mu$mol m$^{-1}$ in the south. Station M11 also strongly affects the distribution pattern of $^3$He in the northern section.

[20] Based on the observed flow field (Figure 3), we have divided the northern inventory into two parts, one that is influenced by the slope current (stations east of M15, red line), and one that is

influenced by the rift valley current (stations west of M15, black line). The $^3$He inventories for the two parts look very similar with 0.48 $\mu$mol m$^{-1}$ for the slope and 0.41 $\mu$mol m$^{-1}$ for the rift valley region. If we assume that the northward component of the slope current of 3.1 cm s$^{-1}$ obtained from the current analyses passes uniformly through the northern slope section, we obtain a $^3$He flux of 0.015 $\mu$mol s$^{-1}$. The southern orientated rift valley current with an average speed southward component of 4.3 cm s$^{-1}$ produces a $^3$He flux of 0.017 $\mu$mol s$^{-1}$. As $^3$He represents a conservative plume tracer, the noticeable similarities between these two sections support the assumption that the slope current transports the vent fluids northward until the plume strikes the southern orientated rift valley current creating a contrarian plume transport (Figure 3). In terms of methane, which is non-conservative, the picture looks quite different. The methane slope and central valley inventories of 31 mol m$^{-1}$ and 9 mol m$^{-1}$, respectively, as well as the associated fluxes of 0.95 mol s$^{-1}$ and 0.37 mol s$^{-1}$, indicate a loss that is presumably related to the microbial oxidation of methane during plume transport (Figure 3).

[21] Assuming that the southward orientated rift valley current (mean current speed of 2.1 cm s$^{-1}$, south component 1.7 cm s$^{-1}$, Figure 2) is finally discharging the plume from the Logatchev vent area, we obtain a $^3$He flux of 0.02 $\mu$mol s$^{-1}$ and a $CH_4$ flux of 0.21 mol s$^{-1}$ through the southern section (Figure 3). Compared with the northern section, the $^3$He fluxes seem to be slightly increased which could be due to an additional plume fraction that is not transported across the northern section, but directly westward into the rift valley.

### 3.4.2. Fluid, $^3$He and Methane Fluxes From Logatchev Vents

[22] To obtain the total flux of the fluids discharged from the Logatchev vent area, we use the $^3$He concentrations that have been analyzed from samples taken by a submerged ROV directly at LHF-1 vent outlets. The mean end-member $^3$He concentration of 22 $\pm$ 6 pM is within the range previously estimated (20–40 pM) from water column data and vent fluid methane concentration [*Keir*, 2010]. According to the $^3$He flux of 0.02 $\mu$mol s$^{-1}$ through the southern section (section 3.4.1), about 900 L s$^{-1}$ of vent fluid is needed to support this horizontal transport. The uncertainty of such an estimate is mainly influenced by the determination of the cross-section inventories [*German et al.*, 2010] and the temporal variability of the horizontal flow field (see chapter 3.1). According to these errors we estimate the flux of vent fluids to be in a range of 900 $\pm$ 400 L s$^{-1}$.

[23] The fluid flux of about 900 L s$^{-1}$ yields a total flux of $CH_4$ of 3.2 mol s$^{-1}$ ([$CH_4$] fluid = 3.5 mM [*Schmidt et al.*, 2007]) which is about three times higher than the flux calculated for the northern slope section (0.95 mol s$^{-1}$; Figure 3). A further decrease of the methane flux can be observed downstream of the source with a final flux across the southern section of 0.21 mol s$^{-1}$ (Figure 3), indicating that about 95% of methane is already oxidized in the near field of that hydrothermal region.

## 4. Conclusion

[24] For the first time current analyses were used to describe the general circulation in the region of Logatchev. This data in combination with the gas distribution pattern was used to deliver a fluid and gas flux estimate from the hydrothermal vents sites. This significant number helps to generate mass balances to describe the transport of matter from the mantel into the hydrosphere, and allows a direct comparison with other hydrothermal sites. Another important result of our study are the indications for an additional vent site that is apparently located northeast of LHF-1. This vent site seems to have an important impact on the gas distribution in the water column as well as on the fluid and gas flux from the hydrothermal region.

## Acknowledgments

[25] We thank the captain, officers and crew aboard R/V *Meteor* M81–2c for their assistance on sea. We gratefully acknowledge the efforts of Peter Wlost, Julia Köhler, Anna Friedrichs, Haugen Grefe and Gregor Halfmann in carrying out the CTD and LADCP work on the cruise. We are also grateful for the support of Dirk Wodarg, Stine Thomas and Jenny Jeschek in building up a GC-C-IRMS line at the IOW for the determination of methane carbon isotopes. We also thank Katja Schmidt for the determination of the concentration of dissolved magnesium in vent-fluid samples. This work was supported by the Deutsche Forschungsgemeinschaft and is publication 68 of the priority program SPP 1144, "From Mantle to the Ocean: Energy-, Material- and Life-cycles at Spreading Axes."

## References

Augustin, N., K. S. Lackschewitz, T. Kuhn, and C. W. Devey (2008), Mineralogical and chemical mass changes in mafic and ultramafic rocks from the Logatchev hydrothermal field (MAR 15°N), *Mar. Geol.*, *256*(1–4), 18–29, doi:10.1016/j.margeo.2008.09.004.

Aumento, F., and H. Loubat (1971), The Mid-Atlantic Ridge near 45°N. XVI. Serpentinized ultramafic intrusions, *Can. J. Earth Sci.*, *8*(6), 631–663, doi:10.1139/e71-062.

Baker, E. T., F. Martinez, J. A. Resing, S. L. Walker, N. J. Buck, and M. H. Edwards (2010), Hydrothermal cooling along the Eastern Lau Spreading Center: No evidence for discharge beyond the neovolcanic zone, *Geochem. Geophys. Geosyst.*, *11*, Q08004, doi:10.1029/2010GC003106.

Batuev, B. N., A. G. Krotov, V. F. Markov, G. A. Cherkashev, S. G. Krasnov, and Y. D. Lisitzin (1994), Massive sulfide deposits discovered at 14°45′N, Mid-Atlantic Ridge, *BRIDGE Newsl.*, *6*, 6–10.

Buller, S. (2008), Methane distribution at Logatchev hydrothermal field at 14°45′N on the Mid-Atlantic Ridge, thesis, 74 pp., Christian-Albrechts Univ., Kiel, Germany.

Cannat, M., et al. (1995), Thin crust, ultramafic exposures, and rugged faulting patterns at the Mid-Atlantic Ridge (22°–24°N), *Geology*, *23*(1), 49–52, doi:10.1130/0091-7613(1995)023<0049:TCUEAR>2.3.CO;2.

Cannat, M., Y. Lagabrielle, H. Bougault, J. Casey, N. de Coutures, L. Dmitriev, and Y. Fouquet (1997), Ultramafic and gabbroic exposures at the Mid-Atlantic Ridge: Geological mapping in the 15°N region, *Tectonophysics*, *279*(1–4), 193–213, doi:10.1016/S0040-1951(97)00113-3.

Charlou, J. L., Y. Fouquet, H. Bougault, J. P. Donval, J. Etoubleau, P. Jean-Baptiste, A. Dapoigny, P. Appriou, and P. A. Rona (1998), Intense CH4 plumes generated by serpentinization of ultramafic rocks at the intersection of the 15°20′N fracture zone and the Mid-Atlantic Ridge, *Geochim. Cosmochim. Acta*, *62*(13), 2323–2333, doi:10.1016/S0016-7037(98)00138-0.

Charlou, J. L., J. P. Donval, Y. Fouquet, P. Jean-Baptiste, and N. Holm (2002), Geochemistry of high $H_2$ and $CH_4$ vent fluids issuing from ultramafic rocks at the Rainbow hydrothermal field (36°14′N, MAR), *Chem. Geol.*, *191*(4), 345–359, doi:10.1016/S0009-2541(02)00134-1.

Charlou, J. L., J. P. Donval, C. Konn, H. Ondréas, Y. Fouquet, P. Jean-Baptiste, and E. Fourré (2010), High production and fluxes of $H_2$ and $CH_4$ and evidence of abiotic hydrocarbon synthesis by serpentinization in ultramafic-hosted hydrothermal systems on the Mid-Atlantic Ridge, in *Diversity of Hydrothermal Systems on Slow Spreading Ocean Ridges*, edited by P. A. Rona et al., *Geophys. Monogr. Ser.*, vol. 188, pp. 265–296, AGU, Washington, D. C., doi:10.1029/2008GM000752.

Di Iorio, D., J. W. Lavelle, P. A. Rona, K. Bemis, G. Xu, L. N. Germanovich, R. P. Lowell, and G. Genc (2012), Measurements and models of heat flux and plumes from hydrothermal discharges near the deep seafloor, *Oceanography*, *25*(1), 168–179, doi:10.5670/oceanog.2012.14.

Dick, H. J. B. (Ed.) (1989), Abyssal peridotites, very slow spreading ridges and ocean ridge magmatism, *Geol. Soc. Spec. Publ.*, *42*, 71–105.

Egbert, G., and S. Erofeeva (2002), Efficient inverse modeling of barotropic ocean tides, *J. Atmos. Oceanic Technol.*, *19*(2), 183–204, doi:10.1175/1520-0426(2002)019<0183:EIMOBO>2.0.CO;2.

Fouquet, Y., et al. (2008), Serpentine cruise–Ultramafic hosted hydrothermal deposits on the Mid-Atlantic Ridge: First submersible studies on Ashadze 1 and 2, Logatchev 2 and Krasnov vent fields, *Interridge News*, *17*, suppl., 16–21.

German, C. R., A. M. Thurnherr, J. Knoery, J. L. Charlou, P. Jean-Baptiste, and H. N. Edmonds (2010), Heat, volume and chemical fluxes from submarine venting: A synthesis of results from the Rainbow hydrothermal field, 36°N MAR, *Deep Sea Res., Part I*, *57*(4), 518–527, doi:10.1016/j.dsr.2009.12.011.

Keir, R. S. (2010), A note on the fluxes of abiogenic methane and hydrogen from mid-ocean ridges, *Geophys. Res. Lett.*, *37*, L24609, doi:10.1029/2010GL045362.

Keir, R. S., O. Schmale, M. Walter, J. Sültenfuß, R. Seifert, and M. Rhein (2008), Flux and dispersion of gases from the "Drachenschlund" hydrothermal vent at 8°18′S, 13°30′W on the Mid-Atlantic Ridge, *Earth Planet. Sci. Lett.*, *270*(3–4), 338–348, doi:10.1016/j.epsl.2008.03.054.

Keir, R., O. Schmale, R. Seifert, and J. Sültenfuß (2009), Isotope fractionation and mixing in methane plumes from the Logatchev hydrothermal field, *Geochem. Geophys. Geosyst.*, *10*, Q05005, doi:10.1029/2009GC002403.

Marbler, H., A. Koschinsky, T. Pape, R. Seifert, S. Weber, E. T. Baker, L. M. de Carvalho, and K. Schmidt (2010), Geochemical and physical structure of the hydrothermal plume at the ultramafic-hosted Logatchev hydrothermal field at 14°45′N on the Mid-Atlantic Ridge, *Mar. Geol.*, *271*(3–4), 187–197, doi:10.1016/j.margeo.2010.01.012.

Petersen, S. (2006), FS Maria S. Merian, HYDROMAR IV, *Cruise Rep. MSM 03-2*, 98 pp., IFM-GEOMAR, Kiel, Germany.

Petersen, S., K. Kuhn, T. Kuhn, N. Augustin, R. Hékinian, L. Franz, and C. Borowski (2009), The geological setting of the ultramafic-hosted Logatchev hydrothermal field (14°45′N, Mid-Atlantic Ridge) and its influence on massive sulfide formation, *Lithos*, *112*(1–2), 40–56, doi:10.1016/j.lithos.2009.02.008.

Petersen, J. M., et al. (2011), Hydrogen is an energy source for hydrothermal vent symbioses, *Nature*, *476*(7359), 176–180, doi:10.1038/nature10325.

Rüth, C., R. Well, and W. Roether (2000), Primordial $^3$He in South Atlantic deep waters from sources on the Mid-Atlantic Ridge, *Deep Sea Res., Part I*, *47*, 1059–1075, doi:10.1016/S0967-0637(99)00077-1.

Schmale, O., S. E. Beaubien, G. Rehder, J. Greinert, and S. Lombardi (2010), Gas seepage in the Dnepr paleo-delta area (NW-Black Sea) and its regional impact on the water column methane cycle, *J. Mar. Syst.*, *80*(1–2), 90–100, doi:10.1016/j.jmarsys.2009.10.003.

Schmidt, K., A. Koschinsky, D. Garbe-Schönberg, L. M. de Carvalho, and R. Seifert (2007), Geochemistry of hydrothermal fluids from the ultramafic-hosted Logatchev hydrothermal field, 15°N on the Mid-Atlantic Ridge: Temporal and spatial investigation, *Chem. Geol.*, *242*(1–2), 1–21, doi:10.1016/j.chemgeo.2007.01.023.

Sudarikov, S. M., and A. B. Roumiantsev (2000), Structure of hydrothermal plumes at the Logatchev vent field, 14°45′N, Mid-Atlantic Ridge: Evidence from geochemical and geophysical data, *J. Volcanol. Geotherm. Res.*, *101*(3–4), 245–252, doi:10.1016/S0377-0273(00)00174-8.

Sültenfuß, J., M. Rhein, and W. Roether (2009), The Bremen Mass Spectrometric Facility for the measurement of helium isotopes, neon, and tritium in water, *Isotopes Environ. Health Stud.*, *45*(2), 1–13.

Tsunogai, U., N. Yoshida, J. Ishibashi, and T. Gamo (2000), Carbon isotopic distribution of mehane in deep-sea hydrothermal plume, Myojin Knoll Caldera, Izu-Bonin arc: Implications for microbial methane oxidation in the oceans and applications to heat flux estimation, *Geochim. Cosmochim. Acta*, *64*(14), 2439–2452, doi:10.1016/S0016-7037(00)00374-4.

Visbeck, M. (2002), Deep velocity profiling using lowered acoustic doppler profilers: Bottom track and inverse solutions,

*J. Atmos. Oceanic Technol.*, *19*(5), 794–807, doi:10.1175/1520-0426(2002)019<0794:DVPULA>2.0.CO;2.

Walker, S. L., E. T. Baker, G. J. Massoth, and R. N. Hey (2004), Short-term variations in the distribution of hydrothermal plumes along a superfast spreading center, East Pacific Rise, 27°30′–32°20′S, *Geochem. Geophys. Geosyst.*, *5*, Q12005, doi:10.1029/2004GC000789.

Walter, M., C. Mertens, U. Stöber, C. R. German, D. R. Yoerger, J. Sültenfuß, M. Rhein, B. Melchert, and E. T. Baker (2010), Rapid dispersal of a hydrothermal plume by turbulent mixing, *Deep Sea Res., Part I*, *57*(8), 931–945, doi:10.1016/j.dsr.2010.04.010.

Welhan, J. A. (1988), Origins of methane in hydrothermal systems, *Chem. Geol.*, *71*(1–3), 183–198, doi:10.1016/0009-2541(88)90114-3.

Whiticar, M. J. (1999), Carbon and hydrogen isotope systematics of bacterial formation and oxidation of methane, *Chem. Geol.*, *161*, 291–314, doi:10.1016/S0009-2541(99)00092-3.